BULLETIN OF THE POLISH ACADEMY OF SCIENCES
TECHNICAL SCIENCES, Vol. 66, No. 1, 2018
DOI: 10.24425/119061

Comparison of heating curves of a rectangular busbar in different conditions of heat abstraction during the short-circuit heating

M. ZARĘBA*

Faculty of Electrical Engineering, Bialystok University of Technology, 45D Wiejska St., 15-351 Bialystok, Poland

Abstract. The paper compares heating curves for a rectangular busbar in the conditions of convective and adiabatic heat transfer during short-circuit heating. Different coefficients of heat transfer from the external surface of the busbar and different busbar cross-sections have been assumed. This has allowed determining the error value occurring when the adiabatic rather than convective boundary condition is presumed at short circuit. The analysis takes into account a change of resistivity in the temperature function. The respective boundary-initial problems have been solved with analytical methods using Green's function. The calculated results show that no considerable errors occur for long-lasting short circuits with an adiabatic rather than convective boundary condition.

Key words: analytical methods of the field theory, transient heat flow, short-circuit in leads, Green's function.

1. Introduction

Thermal field calculations for cables and leads related to short-circuit current flow disregard heat transferred to the environment and treat a heating process as adiabatic [1–3]. It has been recognised that an adiabatic heating process could be presumed for times under one tenth of the time constant of a system [1]. An interesting task is to determine in theory the value of error occurring when this simplification is applied. This error depends on a number of factors (including short-circuit time, busbar's cross-section, cooling conditions) and has an impact on the calculated short-circuit currents.

The aim of this article is to determine the value of error occurring when one presumes the adiabatic rather than convective heat exchange at short circuit. Therefore, heating curves were compared in the aforementioned cases and different variants of the system's operation. The research was carried out for a rectangular busbar with different heat transfer coefficients and different cross-sections. Before short-circuit occurred, it was assumed that the system had had a certain initial temperature distribution resulting from the flow of load current. The analysis was conducted, taking into account a change of resistivity in the temperature function. The respective boundary-initial problems were solved with the use of analytical methods. Green's function was applied especially in cases [4–7]. The main advantage of this approach is that calculation results have the form of formulas, which greatly facilitates the discussion on the impact of the particular parameters as well as the physical interpretation of the results obtained. In the above-mentioned works [4–6], the thermal field was determined by using Green's function in different, simple models, which presumed that heat sources were independent of temperature change or electric current. In this paper, the consideration of variable resistivity resulted in the current-flow-related heat sources being dependent on temperature. This made an analytical result more difficult to obtain.

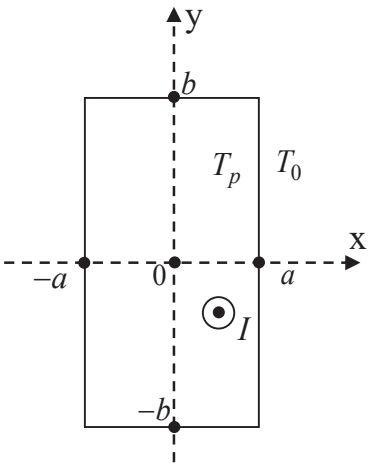

Fig. 1. The cross-section of the rectangular busbar

The object of the research is a rectangular busbar (Fig. 1) heated with direct current DC (I). In Fig. 1 T_0 means ambient temperature and T_p is the initial condition. The system can also be heated with AC current after considering a respective skin factor [1]. In the model under analysis adopted certain simplifying assumptions, not least because of the limitations of the analytical method presented in this paper. It was assumed that the busbar is placed in ambient temperature T_0 and protected against solar radiation. It was also assumed that it is much longer than

*e-mail: m.zareba@pb.edu.pl

Manuscript submitted 2017-01-03, revised 2017-03-16, 2017-05-16, 2017-06-22 and 2017-07-20, initially accepted for publication 2017-08-02, published in February 2018.

its cross-section. The following relation has been established to describe the busbar's variable electric resistivity [8]

$$\rho(T) = \rho(T_0)\big(1 + \varepsilon(T - T_0)\big), \tag{1}$$

where: $\rho(T_0)$ – material's resistivity in temperature T_0, T – temperature, ε – temperature resistivity coefficient. Other busbar's material parameters were assumed as constants (λ – thermal conductivity, c – specific heat, δ – density). With reference to resistivity (1) the aforementioned parameters vary along with temperature to a much lesser extent. The temperature influence coefficients (e.g. for λ and c) are approximately ten and seven times lower, respectively, than in the case of resistivity [9]. When considering the aforementioned parameters' dependence on temperature, the further defined boundary-initial problem becomes nonlinear and obtaining the solution analytically is not possible. In what follows, the heating curves are compared at slightly different temperature values, which will compensate to some extent for nonlinearity of the discussed parameters.

2. Boundary-initial problems of the system

Both of the boundary-initial problems of adiabatic and convective heating differ only in boundary conditions. It is convenient to present these problems with regard to temperature increase $v(x, y, t)$ related to ambient temperature T_0

$$v(x, y, t) = T(x, y, t) - T_0, \tag{2}$$

where: $T(x, y, t)$ – spatial-temporal distribution of temperature field in the busbar, t – time.

The temperature increase (2) in the busbar, with (1) of the previously discussed assumptions applicable, is described by the following heat conduction equation [4]

$$\frac{\partial^2 v(x,y,t)}{\partial x^2} + \frac{\partial^2 v(x,y,t)}{\partial y^2} - \frac{1}{\chi}\frac{\partial v(x,y,t)}{\partial t} + mv(x,y,t) = -\frac{g_0}{\lambda} \quad \text{for } |x| \le a,\ |y| \le b,\ t > 0, \tag{3}$$

where: $m = \dfrac{\rho(T_0)\varepsilon I^2}{16a^2b^2\lambda}$, $\chi = \dfrac{\lambda}{c\delta}$, $g_0 = \dfrac{\rho(T_0)I^2}{16a^2b^4}$,

χ – diffusivity, λ – thermal conductivity, c – specific heat, δ – density, g_0 – efficiency of the spatial heat sources, $2a$ – busbar's width, $2b$ – busbar's height, I – DC current intensity.

In the conditions of convective heat exchange it was assumed that the busbar's surface releases heat by convection and radiation [10, 11]. Hence, the following boundary conditions:

$$\left.\frac{\partial v(x,y,t)}{\partial x}\right|_{x=\pm a} = \mp\frac{\alpha}{\lambda}v(x = \pm a, y, t), \tag{4}$$

$$\left.\frac{\partial v(x,y,t)}{\partial y}\right|_{y=\pm b} = \mp\frac{\alpha}{\lambda}v(x, y = \pm b, t), \tag{5}$$

where α is the total heat transfer coefficient including both convection and radiation.

In the case of adiabatic heating, the boundary conditions are as follows

$$\left.\frac{\partial v(x,y,t)}{\partial x}\right|_{x=\pm a} = \left.\frac{\partial v(x,y,t)}{\partial y}\right|_{x=\pm b} = 0. \tag{6}$$

Before short-circuit current appeared it was assumed that the busbar had a certain initial homogeneous temperature distribution $T_p > T_0$ (Fig. 1). After taking increase (2) into consideration, the initial condition will take the following form

$$v(x, y, t = 0) = T_\mathrm{p} - T_0. \tag{7}$$

Relations (2–5, 7) form the boundary-initial problem with the convective heat exchange, while (2, 3, 6, 7) with the adiabatic heat exchange.

In order to facilitate the solution of the both mentioned-above problems, it is convenient to introduce new function $w(x, y, t)$ [4]

$$v(x, y, t) = w(x, y, t)\cdot e^{m\chi t}. \tag{8}$$

After substituting (8) to (3) the following was obtained

$$\frac{\partial^2 w(x,y,t)}{\partial x^2} + \frac{\partial^2 w(x,y,t)}{\partial y^2} - \frac{1}{\chi}\frac{\partial w(x,y,t)}{\partial t} = -\frac{g_0}{\lambda}e^{-m\chi t} \quad \text{for } |x| \le a,\ |y| \le b,\ t > 0. \tag{9}$$

On the other hand, after considering (8), the form of boundary and initial conditions will not change in either case. Therefore, in order to obtain them, it is sufficient to make change $v(x, y, t) \to w(x, y, t)$ in relations (4–7).

3. Green's functions

Boundary-initial problem of convective heating with regard to $w(x, y, t)$ was solved with the use of Green's function [4–7]. Its basic advantage is the integral form of the solution.

For Green's function $G = G(x, y, t, x', y', \eta)$, the boundary initial problem with regard to $w(x, y, t)$ was defined as follows:

$$\frac{\partial^2 G}{\partial x^2} + \frac{\partial^2 G}{\partial y^2} - \frac{1}{\chi}\frac{\partial G}{\partial t} = -\frac{1}{\chi}\delta(x - x')(y - y')(t - \eta) \quad \text{for } |x| \le a,\ |y| \le b,\ t \le \eta. \tag{10}$$

$$\left.\frac{\partial G}{\partial x}\right|_{x=\pm a} = \mp\frac{\alpha}{\lambda}[G]\Big|_{x=\pm a}, \tag{11}$$

$$\left.\frac{\partial G}{\partial y}\right|_{x=\pm b} = \mp\frac{\alpha}{\lambda}[G]\Big|_{y=\pm b}, \tag{12}$$

$$G = 0 \quad \text{for} \quad t \le \eta, \tag{13}$$

$$G(x, y, t, x', y', \eta) = G(x', y', -\eta, x, y, t), \tag{14}$$

where the right side of (10) is a product of shifted Dirac delta functions (in space after x', y', in time after η). Equation (13) is the causality relation and (14) is the reciprocity of Green's function. According to the physical interpretation, Green's function is a thermal field originating from the above-defined thermal pulse [4, 12].

With the convective heat exchange it could be shown that with the use of (10–14), boundary-initial problem for $w(x, y, t)$ (formulas (9), (4, 5), (7) after change $v(x, y, t) \to w(x, y, t)$), in the second form of Green's theorem [4, 12] one will obtain the following relation [4]

$$w(x, y, t) = (T_p - T_0)\int_{-a}^{a}\int_{-b}^{b} G(x, y, t, x', y', 0)dx'dy' + \\ + \frac{\chi}{\lambda}\int_{0}^{t}\int_{-a}^{a}\int_{-b}^{b} g_0 e^{-m\chi\eta} G(x, y, t, x', y', \eta)dx'dy'd\eta \tag{15}$$

where $G(x, y, t, x', y', 0)$ Green's function for $\eta = 0$.

The first term of relation (15) comes from the initial condition, the second one from the heat sources. Details concerning integral relations with Green's functions for different boundary-initial problems were given, among others in [4, 5, 12].

The aforementioned relation (15) will be the same with adiabatic heating; only Green's function $G(\ldots)$ occurring under integrals signs in (15) will be different.

4. Solution of the boundary-initial problem of convective heating

In order to use (15) one should find Green's function. One of the methods of its determination is to solve the auxiliary problem [12] (without heat sources) by two methods, for instance, separation of variables method [9, 12] and Green's function method defined by means of (10–14). Subsequently, with the respective comparisons of both obtained solutions [4, 12] one may determine Green's function.

Therefore, the following auxiliary problem was discussed with regard to $\Psi(x, y, t)$ This was solved with the separation of variables method and Green's function method

$$\frac{\partial^2\Psi(x, y, t)}{\partial x^2} + \frac{\partial^2\Psi(x, y, t)}{\partial y^2} - \frac{1}{\chi}\frac{\partial^2\Psi(x, y, t)}{\partial t} = 0 \tag{16}$$

for $|x| \le a, \ |y| \le b, \ t > 0,$

$$\left.\frac{\partial\Psi(x, y, t)}{\partial x}\right|_{x=\pm a} = \mp\frac{\alpha}{\lambda}\left[\Psi(x = \pm a, y, t)\right], \tag{17}$$

$$\left.\frac{\partial\Psi(x, y, t)}{\partial y}\right|_{x=\pm b} = \mp\frac{\alpha}{\lambda}\left[\Psi(x, y = \pm b, t)\right], \tag{18}$$

$$\Psi(x, y, 0) = F(x, y) \quad \text{for} \quad |x| \le a, \ |y| \le b, \tag{19}$$

where $F(x, y)$ is the arbitrary distribution of the initial condition.

According to the separation of variables method [10, 12], after separating time and location variables in (16), using boundary conditions (17, 18), and considering the field distribution symmetry in relation to OXY axis, the following was obtained:

$$\psi(x, y, t) = \sum_{k=1}^{\infty}\sum_{n=1}^{\infty} A_{kn}\cos\left(\frac{\beta_k}{a}x\right)\cos\left(\frac{\gamma_n}{b}y\right)e^{-\left(\frac{\beta_k^2}{a^2}+\frac{\gamma_n^2}{a^2}\right)\chi t} \tag{20}$$

for $|x| \le a, \ |y| \le b, \ t > 0.$

where A_{kn} are unknown coefficients and β_k and γ_n are determined by means of the equation of eigenvalues

$$tg(\beta_k) = \frac{\alpha a}{\lambda\beta_{\mathrm{k}}}, \tag{21}$$

$$tg(\gamma_n) = \frac{\alpha b}{\lambda\gamma_{\mathrm{n}}}. \tag{22}$$

Subsequently, in order to determine unknown coefficients A_{kn}, equation (20) was substituted to (19)

$$\sum_{k=1}^{\infty}\sum_{n=1}^{\infty} A_{kn}\cos\left(\frac{\beta_k}{a}x\right)\cos\left(\frac{\gamma_n}{b}y\right) = F(x, y) \tag{23}$$

for $|x| \le a, \ |y| \le b.$

Equation (23) was multiplied by $\cos\left(\frac{\beta_i}{a}x\right)$ and $\cos\left(\frac{\gamma_l}{b}y\right)$ and the relations obtained in that way were integrated with respect to coordinate x in the range $\langle -a, a\rangle$ and with respect to y in the range $\langle -b, b\rangle$. After using the orthogonality of trigonometric functions in the discussed ranges, the following was obtained

$$A_{kn} = \frac{\int_{-a}^{a}\int_{-b}^{b} F(x, y)\cos\left(\frac{\beta_k}{a}x\right)\cos\left(\frac{\gamma_n}{b}y\right)dxdy}{ab\left(1 + \frac{\alpha a}{\beta_k^2\lambda}\cos^2(\beta_k)\right)\left(1 + \frac{\alpha b}{\gamma_n^2\lambda}\cos^2(\gamma_n)\right)}. \tag{24}$$

After making the change under the integrals $x \to x'$, $y \to y'$ in (24) and substituting (24) to (20) and proper ordering, the following was obtained

$$\Psi(x, y, t) = \\ = \int_{-a}^{a}\int_{-b}^{b}\sum_{k=1}^{\infty}\sum_{n=1}^{\infty}\frac{\cos\left(\frac{\beta_k}{a}x'\right)\cos\left(\frac{\beta_k}{a}x\right)\cos\left(\frac{\gamma_n}{b}y'\right)\cos\left(\frac{\gamma_n}{b}y\right)}{ab\left(1 + \frac{\alpha a}{\beta_k^2\lambda}\cos^2(\beta_k)\right)\left(1 + \frac{\alpha b}{\gamma_n^2\lambda}\cos^2(\gamma_n)\right)} \\ e^{-\left(\frac{\beta_k^2}{a^2}+\frac{\gamma_n^2}{a^2}\right)\chi t} F(x', y')dx'dy'. \tag{25}$$

On the other hand, the solution of the auxiliary problem (16–19) expressed with Green's function comes only from non-zero initial distribution $F(x, y)$ and it is in the form of

$$\Psi(x, y, t) = \int_{-a}^{a}\int_{-b}^{b} G(x, y, t, x', y', \eta = 0)F(x', y')dx'dy', \quad (26)$$

where $G(x, y, t, x', y', 0)$ - Green's function for $\eta = 0$.

After a proper comparison of (26) and (25), change $t \to t - \eta$ [4, 12], Green's function was obtained

$$G(x, y, t, x', y', \eta) = \\ = \frac{1}{ab}\sum_{k=1}^{\infty}\sum_{n=1}^{\infty}\frac{\cos\left(\frac{\beta_k}{a}x'\right)\cos\left(\frac{\beta_k}{a}x\right)\cos\left(\frac{\gamma_n}{b}y'\right)\cos\left(\frac{\gamma_n}{b}y\right)}{\left(1+\frac{\alpha a}{\beta_k^2\lambda}\cos^2(\beta_k)\right)\left(1+\frac{\alpha b}{\gamma_n^2\lambda}\cos^2(\gamma_n)\right)} \quad (27)$$
$$e^{-\chi(t-\eta)\left(\frac{\beta_k^2}{a^2}+\frac{\gamma_n^2}{a^2}\right)} \quad \text{for} \quad |x| \le a,\ |y| \le b,\ t > \eta.$$

Figure 2 shows an example of the time-profiles of Green's function (27) in point $(x, y) = (a, b)$ for the case of thermal pulse generation in point $(x, y) = (0, 0)$ at $\eta = 1000$ s for various heat transfer coefficients α. The data essential to draw up Fig. 2 were taken from set (35).

Finally, after substituting Green's function (27) to (15) and calculating the relevant integrals, taking account of (8) and (2), the following heating curves were obtained:

$$T_K(x, y, t) = T_0 + 4(T_p - T_0)\cdot\sum_{k=1}^{\infty}\sum_{n=1}^{\infty}A_{kn}(x, y)\cdot \\ \cdot e^{-\chi t\left[\left(\frac{\beta_k^2}{a^2}+\frac{\gamma_n^2}{a^2}\right)-m\right]} + \frac{4g_0a^2b^2}{\lambda}\cdot\sum_{k=1}^{\infty}\sum_{n=1}^{\infty}\frac{A_{kn}(x, y)}{\xi_{kn}}\cdot \quad (28) \\ \cdot\left(1 - e^{-\chi t\left[\left(\frac{\beta_k^2}{a^2}+\frac{\gamma_n^2}{a^2}\right)-m\right]}\right),$$

where:

$$A_{kn}(x, y) = \frac{\cos\left(\frac{\beta_k}{a}x\right)\cos\left(\frac{\gamma_n}{b}y\right)\sin(\beta_k)\sin(\gamma_n)}{\left(\beta_k+\frac{\alpha a}{\beta_k\lambda}\cos^2(\beta_k)\right)\left(\gamma_n+\frac{\alpha b}{\gamma_n\lambda}\cos^2(\gamma_n)\right)}, \quad (29)$$

$$\xi_{kn} = \beta_k^2b^2 + \gamma_n^2a^2 - ma^2b^2, \quad (30)$$

and eigenvalues β_k and γ_n are determined from equations (21, 22).

One should also determine the thermal time constant of the system which is useful when determining the time of comparing heating curves. In order to calculate that constant, the criterion of an average (local) time constant was used [13, 14]

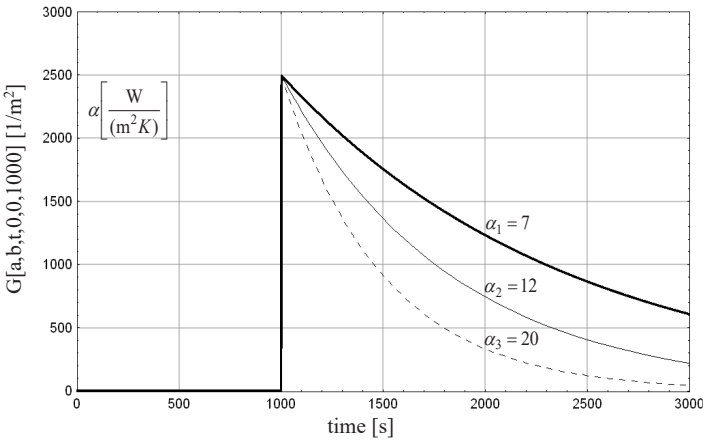

Fig. 2. Green's function (27) diagrams $G(x = a, y = b, t, x' = 0, y' = 0, \eta = 1000)$ for various heat transfer coefficients in the busbar for cross-section $S_2 = 400\ \text{mm}^2$

$$\tau(x, y) = \int_0^{\infty}\frac{T_k(x, y, t) - T_s(x, y)}{T_k(x, y, t = 0) - T_s(x, y)}dt, \quad (31)$$

where $T_s(x, y)$ is the stationary distribution determined from (28) with $t \to \infty$.

After substituting (28) to (31) as well as integrating and reducing, the average time constant of the busbar was obtained

$$\tau(x, y) = \\ = \frac{4(T_p - T_0)\sum_{k=1}^{\infty}\sum_{n=1}^{\infty}\frac{A_{kn}(x, y)a^2b^2}{\chi\xi_{kn}} - \frac{4g_0a^2b^2}{\lambda}\sum_{k=1}^{\infty}\sum_{n=1}^{\infty}\frac{A_{kn}(x, y)a^2b^2}{\chi\xi_{kn}^2}}{4(T_p - T_0)\sum_{k=1}^{\infty}\sum_{n=1}^{\infty}A_{kn}(x, y) - \frac{4g_0a^2b^2}{\lambda}\sum_{k=1}^{\infty}\sum_{n=1}^{\infty}\frac{A_{kn}(x, y)}{\xi_{kn}}} \quad (32)$$

for $|x| \le a, \quad |y| \le b,$

where $A_{kn}(x, y)$ and ξ_{kn} are described by equation (29) and (30).

5. Solution of the boundary-initial problem of adiabating heating

Adiabatic heating temperature distribution can also be obtained by using Green's function in the same way as in the case of convective heating. However, a more convenient method of obtaining the solution is to use limiting case $(\alpha \to 0)$ which changes convective boundary conditions (4, 5) into adiabatic ones (6). The aforementioned limiting case is applied to final relations (21, 22) and (28), which describe temperature distribution with convective heating. Therefore, equations of eigenvalues were obtained from (21, 22) with $\alpha \to 0$:

$$\sin(\beta_k) = \sin(\gamma_n) = 0 \quad (33)$$

where first eigenvalues are zero (that is $\beta_0 = \gamma_0 = 0$). Subsequently, after substituting (33) to (28–30), all the terms of the

series are zeroed except for the first components related to zero eigenvalues which will be indeterminate forms. As a result, after using L'Hôpital's rule for $\beta_0 = \gamma_0 = 0$ from (28), one obtains temperature changes with adiabatic heating

$$T_A(t) = T_0 + (T_p - T_0)e^{m\chi t} + \frac{g_0}{m\lambda}\left(e^{m\chi t} - 1\right), \tag{34}$$

where $T_A(t)$ – heating curves in adiabatic conditions.

6. Computational examples

Mathematica software [15, 16] was used to calculate heating curves with convective (28) and adiabatic (34) boundary conditions as well as time constants (32). The computational example was a rectangular aluminium busbar. The following data were assumed:

$$\begin{aligned} &T_0 = 20°\text{C}, \;\; T_p = 40°\text{C}, \;\; \lambda = 229 \text{ W/(mk)}, \\ &c = 910 \text{ J/(kgK)}, \;\; \delta = 2720 \text{ kg/m}^3, \\ &\rho = \left(T_0 = 20°\text{C}\right) = 2.8264 \cdot 10^{-8} \,\Omega\text{m}, \\ &\varepsilon = 40.3 \cdot 10^{-4} \text{ 1/k}. \end{aligned} \tag{35}$$

What is more, the calculations were made for three different cross-sections of the busbar $S_1 = 100 \text{ mm}^2$ with current $I_1 = 0.8$ kA, $S_2 = 400 \text{ mm}^2$ with $I_2 = 3$ kA and $S_3 = 900 \text{ mm}^2$ with $I_3 = 7$ kA. In all the above-mentioned cases, a constant ratio for busbar dimensions was adopted as $b/a = 4$. Moreover, three different heat transfer coefficients were assumed: $\alpha_1 = 7 \text{ W/(m}^2\text{K)}$, $\alpha_2 = 12 \text{ W/(m}^2\text{K)}$ and $\alpha_3 = 20 \text{ W/(m}^2\text{K)}$. With regard to a fast convergence of series in (28), only 25 terms of each sum were considered in (28).

In order to determine the error value of replacing the convective condition with the adiabatic one, the relative differences of heating curves were analysed according to the following relation

$$100\% \, \frac{T_A(t) - T_K(x, y, t)}{T_K(x, y, t)}. \tag{36}$$

Due to aluminium's considerable thermal conductivity, the results of calculations were presented for one point of coordinates $x, y) = (a, b)$. Figure 3 shows heating curves with the convective (28) and adiabatic boundary condition (34) in the busbar for $S_2 = 400 \text{ mm}^2$ and $I_2 = 3$ kA with different heat transfer coefficients. On the other hand, Fig. 4 shows relative differences of heating curves (36) in the busbar for $S_2 = 400 \text{ mm}^2$ and $I_2 = 3$ kA also for different heat transfer coefficients. Figure 5 shows relative differences (36) with constant $\alpha_2 = 12 \text{ W/(m}^2\text{K)}$ but with different cross-sections of the busbar for different currents I (for data mentioned under data set (35)). Also Table 1 lists calculations of relative difference values (36) for one tenth of the time constant. In order to calculate the time constant, (32) was used.

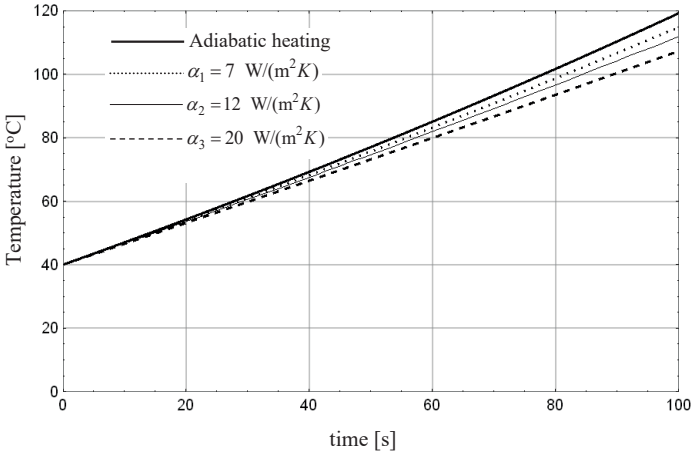

Fig. 3. Heating curves in the busbar in adiabatic and convective conditions with cross-section $S_2 = 400 \text{ mm}^2$ for short-circuit current $I_2 = 3$ kA

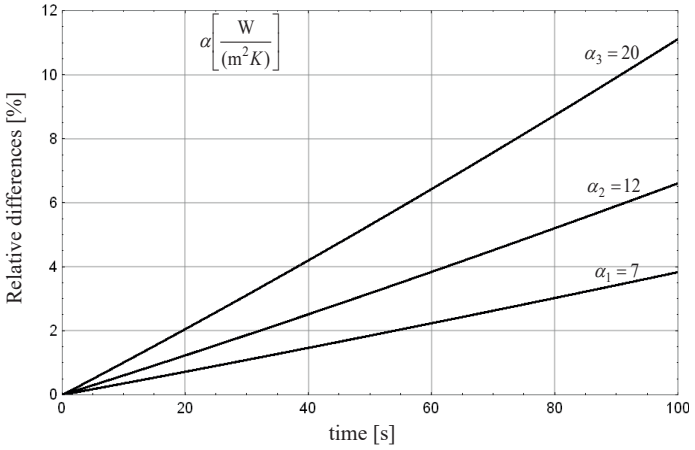

Fig. 4. Relative differences of heating curves (36) in adiabatic and convective boundary conditions with different heat transfer coefficients for $S_2 = 400 \text{ mm}^2$ and short-circuit current $I_2 = 3$ kA

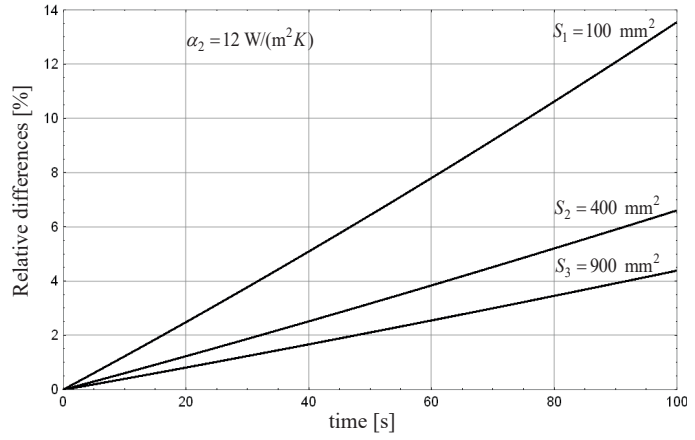

Fig. 5. Relative differences of heating curves (36) in adiabatic and convective boundary conditions with different cross-sections for: $S_1 = 100 \text{ mm}^2$ and $I_1 = 0.8$ kA, $S_2 = 400 \text{ mm}^2$ and $I_2 = 3$ kA, $S_3 = 900 \text{ mm}^2$ and $I_3 = 7$ kA

Table 1
Values of relative differences (36) for one tenth of the time constant with different heat transfer coefficient and different cross-sections of the busbar

cross-section S [mm^2]	heat transfer coefficent α [W/(m^{2}K)]	value of 1/10 time constant 0.1 τ[a, b] [s]	relative differences for 0.1 τ[a, b] [%]
100	12	57.2	7.4
400	12	113.1	7.55
900	12	174.2	8
400	7	195.7	7.95
400	12	113.1	7.55
400	20	66.9	7.21

In order to verify analytical relations (28) and (34), the boundary-initial problems of convective and adiabatic heating were solved again by the finite element method [17, 18]. A two-dimensional model (Fig. 1) was approximated by a mesh consisting of 40 000 square elements (100×400). The temperature distribution in each of the elements was approximated by the linear combination of second-order polynomials. The calculations were made in Mathematica software [15] with 10^{-6} accuracy for a busbar with $S_2 = 400$ mm^2 cross-section, short-circuit current $I_2 = 3$ kA with $\alpha_2 = 12$ W/(m^{2}K). As a result, Fig. 6 shows temperature differences between heating curves obtained by means of the finite element method and the method presented in the paper for adiabatic and convective heating, that is

$$T_{AN}(t) - T_A(t), \tag{37}$$

$$T_{KN}(a, b, t) - T_K(a, b, t), \tag{38}$$

where: $T_{AN}(t)$, $T_{KN}(a, b, t)$ – heating curves in the adiabatic and the convective conditions calculated by means of the finite element method,

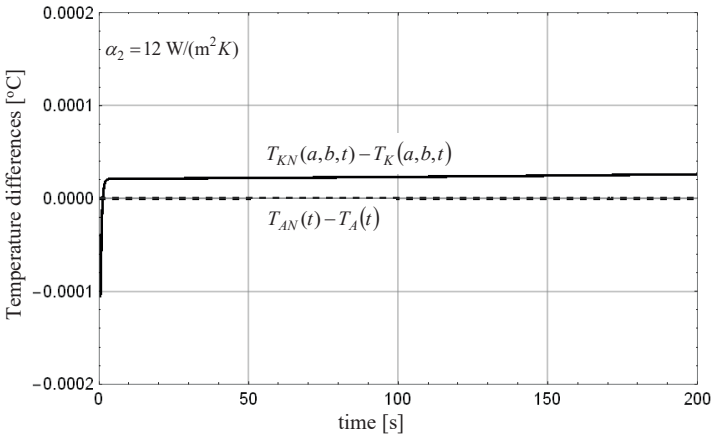

Fig. 6. Differences of heating curves $T_{KN}(a, b, t) - T_K(a, b, t)$ and $T_{AN}(t) - T_A(t)$ determined with analytical and numerical methods in the busbar for cross-section $S_2 = 400$ mm^2 with short-circuit current $I_2 = 3$ kA and $\alpha_2 = 12$ W/(m^{2}K)

$T_{AN}(t)$, $T_{KN}(a, b, t)$ – heating curves in the adiabatic and the convective conditions calculated by means of the method presented in the paper.

The impact of mesh density used in the finite element method on the above-defined differences (37, 38) was also investigated. Therefore, Table 2 shows the differences (37, 38) for several selected time moments at three different mesh sizes. From the table presented, it can be seen that the mesh size has a negligible effect on errors (37, 38). This is due to the high thermal conductivity of the busbar ($\lambda = 229$ W/(mK)), and this makes the spatial temperature drop small. It is worth adding that the effect of the mesh density is significant at high temperature drop.

Table 2
Temperature difference values (37, 38) obtained from comparison of analytical and numerical methods for selected time moments and different mesh sizes

temperature differences $T_{KN}(a, b, t) - T_K(a, b, t)$			
mesh size	t = 10 s	t = 50 s	t = 200 s
5×20	0.000021219	0.000021964	0.000026092
10×40	0.000021224	0.000021968	0.000026095
20×80	0.000021225	0.000021997	0.0000261
temperature differences $T_{AN}(t) - T_A(t)$			
mesh size	t = 10 s	t = 50 s	t = 200 s
5×20	$6.8241 \cdot 10^{-9}$	$7.7641 \cdot 10^{-9}$	$1.3111 \cdot 10^{-8}$
10×40	$6.785 \cdot 10^{-9}$	$7.4081 \cdot 10^{-9}$	$9.3953 \cdot 10^{-9}$
20×80	$6.8514 \cdot 10^{-9}$	$8.0376 \cdot 10^{-9}$	$1.6734 \cdot 10^{-8}$

7. Results

A) Short heating with short-circuit current makes the heating curves for shorter times almost linear and practically overlapping both in the adiabatic and convective conditions (Fig. 3). However, for longer times, there is a clear separation of the mentioned curves, especially with the increasing heat transfer coefficient (Fig. 3). This is related to the process of cooling in the conditions of convective heat exchange, causing the busbar to be heated to lower temperature (dependent on the heat transfer coefficient) than in adiabatic conditions. Also Fig. 4 shows that higher values of heat transfer coefficient lead to higher values of relative differences (36) between heating curves. With the constant heat transfer coefficient and the decreasing cross-section of the busbar, the increase in the values of relative differences is also observed (36) (Fig. 5). With the value of one tenth of the time constant (Table 1), the values of relative difference (36) for different variants of change α and cross-section S are in the range of 7.2–8%. The fact that the value of the time constant (Table 1) depends on the cross-section of the busbar and the heat transfer coefficient is worth mentioning here. For instance, with a constant cross-section of the busbar, higher values of

heat transfer coefficient give lower values of time constants. This is also visible in Fig. 2, where faster drops of Green's function are observed at higher values of heat transfer coefficient. A significant parameter of cables and leads is the one-second density of the short-circuit current [2], which is usually determined up to 5 s. In these conditions, values of (36) do not exceed 0.6% in the worst case.

B) In both the adiabatic and the convective boundary conditions, temperature distribution differences (calculated with the finite element method and analytical method) are very small (Fig. 6).

8. Conclusion

The above results, in particular Table 1, suggest that adopting an adiabatic rather than a convective condition does not produce a greater error even for a short-circuit current of considerable duration (up to one tenth of the time constant). Furthermore, with regard to the aforementioned inconsiderable errors, relatively simple relation (34) with adiabatic heating may also be used in the conditions of irregular or interceptive regime [2] of busbars.

With regard to very small errors of the presented method in relation to the finite element method (Fig. 6), solution of (28) and (34) can be considered as a verified one.

Acknowledgements. The paper was prepared at the in Białystok University of Technology within the framework of the project S/WE/01/13 sponsored by the Ministry of Science and Higher Education.

References

[1] S. Kulas, *Current Ducts and Contact Systems*, Warsaw University of Technology Publishing House, Warsaw, 2008, [in Polish].

[2] H. Markiewicz, *Electric Power Devices*, WNT, Warsaw, 2016, [in Polish].

[3] J. Maksymiuk and Z. Pochanke, *Computation and Diagnostic Investigations of Power Distributing Apparatus*, WNT, Warsaw, 2001, [in Polish].

[4] K.D. Cole, A. Haji-Sheikh, J.V. Beck, and B. Litkouhi, *Heat Conduction Using Green's Functions*, CRC Press, 2011.

[5] D.G. Duffy, *Green's Function with Applications*, CRC Press, 2015.

[6] M.D. Greenberg, *Applications of Green's Function in Science and Engineering*, Dover Publications, USA, 2015.

[7] K. Gnidzinska, G. de Mey, and A. Napieralski, "Heat dissipation and temperature distribution in long interconnect lines", Bull. Pol. Ac.: Tech. 58 (1), 119–124, (2010).

[8] G.J. Anders, *Rating of Electric Power Cables: Ampacity Computations for Transmission, Distribution, and Industrial Applications*, McGraw-Hill Professional, New York, 1997.

[9] N.W. Ashcroft and N.D. Mermin, *Solid State Physics*, Holt-Saunders International Editions, Japan, 1981.

[10] M.J. Latif, *Heat Conduction*, Springer-Verlag, Haidelberg, 2009.

[11] M.D. Baehr and K. Stephan, *Heat and Mass Transfer*, Springer-Verlag, Heidelberg, 2006.

[12] D.W. Hahn and M.N. Ozisik, *Heat Conduction*, John Wiley & Sons, New Jersey, 2012.

[13] A. Brykalski, "Ein Beitrag zur Bestimmung der mittleren Zeitkonstante von Diffusionsprozessen", *International Journal of Heat and Mass Transfer* 28 (3), 13–620 (1985).

[14] W. Lipiński and J. Golębiowski, "Modeling of electromagnetic shield dynamics", *IEEE Transactions on Magnetics* 16 (6), 1419–1422 (1986).

[15] P. Wellin, *Essentials of Programming in Mathematica*, Cambridge University Press, UK, 2014.

[16] Wolfram Research, Inc., *Mathematica*, Version 10.4, Champaign, IL, 2016.

[17] S. Brenner and R.L. Scott, *The Mathematical Theory of Finite Element Methods*, Springer, Berlin, 2008.

[18] K.J. Bathe, *Finite-Elemente Methoden*, Springer-Verlag, Berlin, 1990.